The Meteoritical Society

Meteoritics & Planetary Science 52, Nr 12, 2695–2706 (2017)
doi: 10.1111/maps.12987

The origin of alteration "orangettes" in Dhofar 019: Implications for the age and aqueous history of the shergottites

L. J. HALLIS[1*], L. KEMPPINEN[1,3], M. R. LEE[1], and L. A. TAYLOR[2]

[1]School of Geographical and Earth Science, University of Glasgow, Glasgow G12 8QQ, Scotland, UK
[2]Department of Earth and Planetary Sciences, University of Tennessee, Knoxville, Tennessee 37996–1410, USA
[3]Present address: School of Earth Sciences, University of Bristol, Clifton BS8 1RJ, UK
[*]Corresponding author. E-mail: lydia.hallis@glasgow.ac.uk

(Received 04 February 2016; revision accepted 30 August 2017)

Abstract–The shergottites are the largest group of Martian meteorites, and the only group that has not been found to contain definitive evidence of Martian aqueous alteration. Given recent reports of current liquid water at the surface of Mars, this study aimed to investigate in detail the possibility of Martian phyllosilicate within shergottite Dhofar 019. Optical and scanning electron microscopy, followed by transmission electron microscopy, confirmed the presence of alteration orangettes, with a layered structure consisting of poorly ordered Mg-phyllosilicate and calcite. These investigations identified maskelynite dissolution, followed by Mg-phyllosilicate and calcite deposition within the dissolution pits, as the method of orangette production. The presence of celestine within the orangette layers, the absence of shock dislocation features within calcite, and the Mg-rich nature of the phyllosilicate, all indicate a terrestrial origin for these features on Dhofar 019.

INTRODUCTION

The 1.056 kg mass of Dhofar 019 was found in the Oman desert on January 24, 2000 (Grossman 2000) and is classified as an olivine-phyric basaltic shergottite. Its modal mineralogy is estimated as ~64% clinopyroxene, ~9% olivine, and ~25% maskelynite (Borg et al. 2001). Accessory minerals include silica, potassium-rich feldspar, whitlockite, chlorapatite, chromite, ilmenite, magnetite, and pyrrhotite (Shukolyukov et al. 2002). Based on incompatible trace element depletion, Dhofar 019 is classified as a depleted endmember of the shergottite group (Brandon et al. 2008, 2012).

Crystallization ages of 525 ± 56 Ma, 575 ± 7 Ma, and 540 ± 20 Ma have been reported, based on Rb/Sr, Sm/Nd, and K/Ar data, respectively (Borg et al. 2001; Shukolyukov et al. 2002). These ages are old relative to most other shergottites (165–475 Ma; e.g., Nyquist et al. 2001), but roughly correspond to the age of Tissint (574 ± 20 Ma; Brennecker et al. 2014). Based on their similar cosmic-ray exposure ages, it had been suggested that all depleted olivine-phyric shergottites are launch-paired (Nishiizumi et al. 2012), but Dhofar 019 does not fit into this model. A maximum cosmic-ray exposure age of 20 Ma for Dhofar 019 is 5 Ma longer than the previously assumed oldest Martian meteorite exposure age of 15 Ma obtained from Allan Hills (ALH) 84001 (Shukolyukov et al. 2002). Therefore, either Dhofar 019 is unique among the Martian meteorites, having been launched from a separate site on Mars at an earlier date, or terrestrial contamination has affected the results of cosmic-ray exposure measurements.

As Dhofar 019 was subaerially exposed to a hot desert environment for 0.34 ± 0.04 Ma (Nishiizumi et al. 2002), it has experienced terrestrial weathering and erosion. Most obviously, the fusion crust has been eroded via aeolian abrasion (Grossman 2000). The stone was found partially buried in caliche soil, resulting in the formation of veins of terrestrial calcite, along with gypsum, phyllosilicate (reported as smectite), celestine, and iron hydroxide, throughout the meteorite (Grossman 2000; Shukolyukov et al. 2002; Taylor et al. 2002). Olivine grains have a distinctive rust-brown coloration due to the presence of Fe-hydroxide veins

within cracks and along their edges (Taylor et al. 2002). Spherical structures, referred to as orangettes, are also present in Dhofar 019 (Grossman 2000). These orangettes are concentrically zoned with respect to their chemical composition and mineralogy, with smectite, calcite, and (rarely) gypsum layers. They occur enclosed within the matrix feldspathic glass and at its contacts with large pyroxene grains. These distinctive orangettes bear a superficial resemblance to the widely studied preterrestrial carbonate assemblages in ALH 84001 (e.g., Mason et al. 1992; Mittlefehldt and Lindstrom 1994; Treiman and Romanek 1998; Scott 1999). The ALH 84001 carbonate rosettes are, however, different from those in Dhofar 019 in that they are composed of Fe- and Mg-rich carbonates with magnetite.

The nakhlites are known to contain relatively abundant Martian alteration minerals, including Fe-rich saponite and serpentine, siderite carbonate, and sulfates (e.g., Gooding et al. 1991; Romanek et al. 1994; Treiman and Romanek 1998; Bridges and Grady 2000; Changela and Bridges 2011; Hallis and Taylor 2011; Hicks et al. 2014). Chassigny is reported to contain Martian carbonates and sulfate (Wentworth and Gooding 1994), and as mentioned above, ALH 84001 contains preterrestrial carbonate rosettes. These phases are known to be preterrestrial as they are altered by the formation of, and incorporated into, the fusion crust (e.g., Gooding et al. 1991; Hallis 2013). In addition, mineral offsetting due to the formation of impact shock fractures (e.g., when the meteorite leaves Mars) is commonly seen in Martian alteration assemblages. Oxygen isotope analyses of water from polymict breccia Northwest Africa (NWA) 7034 have been used to suggest its ferrous iron oxides, and hydroxides have a Martian origin (Agee et al. 2013; Muttik et al. 2014). Thus, the shergottites—despite being by far the largest group of Martian meteorites—are conspicuous as potentially the only group that lack products of Martian aqueous alteration. This absence may be explained by their young age. Over geological time, the Martian surface has dried out dramatically. The shergottites crystallized <600 Myr ago on Mars (although this is debated by some [see Bouvier et al. 2008]). In contrast, the nakhlites crystallized at 1.3 Ga and ALH 84001 at >4 Ga (Nyquist et al. 2001). Therefore, by the time the shergottites crystallized, the Martian surface was relatively dry. However, it remains possible that the shergottites were exposed to aqueous fluids on Mars. Remote-sensing images have revealed the presence of recurrent slope lineae, thought to be formed by aqueous brines at the Martian surface (McEwen et al. 2011; Ojha et al. 2015). In addition, a number of recently formed gullies are reported to be produced via the melting of water-rich snow deposits (Christensen 2003). These formations prove that, even now, the Martian surface is not completely dry.

Taylor et al. (2002) found that smectite in at least one Dhofar 019 orangette appears to have been displaced by shock fracturing through maskelynite, suggesting that some of the smectite may be preterrestrial. This finding is significant, as it is the most substantiated report of possible preterrestrial alteration in the shergottite meteorites. The aim of this study was to determine whether any of the material in the alteration orangettes of Dhofar 019 has a preterrestrial origin. If so, this meteorite would be a very important source of evidence for relatively recent Martian groundwater. To achieve this aim, we searched for shock features in the orangettes of Dhofar 019, thin-section 610-A, and compared the orangette compositions to known Martian alteration assemblages.

METHODS

Sample Imaging and Chemical Classification of Target Phases

In addition to optical microscopy, the Carl Zeiss Sigma Variable Pressure Analytical SEM and the FEI Quanta 200F Environmental SEM were utilized in backscattered electron (BSE) mode to locate areas of interest (AOI) within Dhofar 019 thin-section 610-A. Energy-dispersive X-ray analysis (EDX) was used to characterize separate layers within the orangettes. AOIs 1 and 2 were selected on the basis of the large orangette size and the presence of multiple layers. Quantitative X-ray analysis was undertaken using a Zeiss Sigma analytical SEM, equipped with an Oxford Instruments X-Max silicon-drift X-ray detector, operated through an AZTEC microanalysis system. Quantitative analyses were acquired at 20 kV and 3 nA, with the beam current regularly measured using a Faraday cup. X-ray spectra were collected for 60 s, and quantified with reference to the following mineral standards that were obtained from the supplier, P&H Developments Ltd: jadeite (Na), periclase (Mg), corundum (Al), diopside (Si), apatite (P), pyrite (S), K-feldspar (K), wollastonite (Ca), rutile (Ti), chromite (Cr), rhodonite (Mn), garnet (Fe), and Ni-metal (Ni). Typical detection limits (in wt%) were Na (0.08), Mg (0.05), Al (0.08), Si (0.04), P (0.06), S (0.06), K (0.09), Ca (0.06), Ti (0.11), Cr (0.12), Mn (0.12), Fe (0.22), and Ni (0.17). This quantitative X-ray analysis method was also used by Tomkinson et al. (2013).

Focused Ion Beam Section Preparation and Transmission Electron Microscope Analysis

To enable transmission electron microscope (TEM) analysis, two electron-transparent focused ion beam

(FIB)-sections were cut from the surface of thin-section 610-A. The sections were prepared using a FEI Duomill dual-beam FIB instrument operated with a 30 kV Ga^+ ion beam and following the procedure of Lee et al. (2003). Prior to milling, the AOI was capped with a 15 μm long by 4 μm wide and 0.1 μm thick layer of Pt that was applied using a gas injection system and deposited by interaction with the electron beam. Initially, each foil was ion-milled to a thickness of approximately 1 μm, using high (~1 nA) beam currents. Following its in situ extraction, the thick foil was welded to the tines of a copper holder using electron- and ion beam-deposited Pt and reduced to approximately 100 nm thickness at lower current (~100 pA).

Bright-field and dark-field diffraction-contrast images and selected area electron-diffraction (SAED) patterns were acquired from the FIB-sections using a FEI T20 TEM operated at 200 kV. Bright-field and high-angle annular dark-field (HAADF) scanning TEM (STEM) imaging was also performed using a JEOL ARM200cF MagTEM operated at 200 kV. This microscope is equipped with a Gatan Quantum electron spectrometer for major and minor element quantitative EDX analysis. EDX conditions included a 0.4–0.6 nm spot size and 100 pA current on the sample, at 200 kV with a 40 μm condenser aperture. The count time for each analysis was 30 s. X-ray spectra were quantified via a standardless procedure using the Cliff–Lorimer correction.

RESULTS

Alteration in Dhofar 019

An initial search of thin-section 610-A revealed the extensive nature of terrestrial weathering within Dhofar 019. Caliche soil adheres to one edge of the sample (Fig. 1a), with a sharp boundary between the soil and meteorite (Fig. 1b). The sample is entirely penetrated by calcite veins running through fractures in clinopyroxene and olivine grains (Figs. 1b, 1c, 2a, and 2b), but these veins are more abundant toward the caliche-covered edge. Deposits of celestine ($SrSO_4$) and barite ($BaSO_4$) only occur within 3 mm of the adhering caliche soil (Figs. 1b, 2a, and 2d). The opposite edge appears to have been exposed to more erosive weathering. Some clinopyroxene dissolution has occurred along this edge, following cleavage planes. More commonly, the dissolution is concentrated along the boundaries of clinopyroxene or olivine with maskelynite (Fig. 1c). Optical microscopy reveals olivine grains are largely rust-brown due to the presence of Fe-hydroxide veins along internal cracks. Olivine alteration areas consisting of an Mg-rich phase are also evident in several grains (Fig. 1b). Dissolved maskelynite is commonly only partially replaced by secondary minerals, leaving a void between the unaltered maskelynite and the bounding mineral. This void space, which can be up to 100 μm wide, may result from preferential removal of secondary phases during sample preparation. However, the delicate texture of the phases that are present argue against this. Instead, it seems more likely that maskelynite was first dissolved and later these void spaces were infilled. Where the void space is completely filled, the boundary between maskelynite and the secondary assemblage is commonly diffuse (Figs. 1d–g), with phyllosilicate replacing maskelynite. Other phases within the secondary assemblage include calcite, celestine, barite (close to the caliche soil edge), and rare gypsum (Table 1).

Numerous orangettes were located in thin-section 610-A (Fig. 2). Texturally these differ from the previously described alteration in that they are layered spherical structures (<50 μm diameter). However, mineralogically, the layers are made up of calcite and Mg-rich phyllosilicate of the same composition found within the larger void-filling areas of alteration. Numerous hemispherical layered orangettes are present at the boundaries of clinopyroxene with maskelynite. A number of these hemispherical structures within 400 μm of the caliche soil edge contain celestine or barite as one of the layers.

Hemispherical dissolution pits are present along fractures in maskelynite at the surface of thin-section 610-A (Fig. 3). The fractures may have been produced during the ejection impact event that caused plagioclase to convert to maskelynite, or by the impact of the meteorite hitting the Earth's surface. They commonly cut through and offset primary mineral inclusions within maskelynite, such as phosphate or magnetite. However, in sample 610-A, no definitive example of orangette offsetting was found. Secondary phases were observed within the fractures and pits, including gypsum, Fe-oxide, and Mg-phyllosilicate. Some pits exhibit ragged edges and contain Mg-rich phyllosilicate that has grown across the central fracture (Figs. 3a and 3c), indicating it must have been deposited after fracturing occurred. In one case (Fig. 3a), the onset of a layered structure was observed. In cases where hemispherical dissolution pits have grown on either side of a fracture (Figs. 3b and 3d), the illusion of offsetting is produced, but closer observation reveals that the number and amount of offset does not match up on both sides of the fracture.

Small-Scale Analysis of Orangettes

FIB-sections 1 and 2 were cut from orangettes that were selected for study, owing to the presence of multiple layers of calcite and phyllosilicate (Figs. 2a and

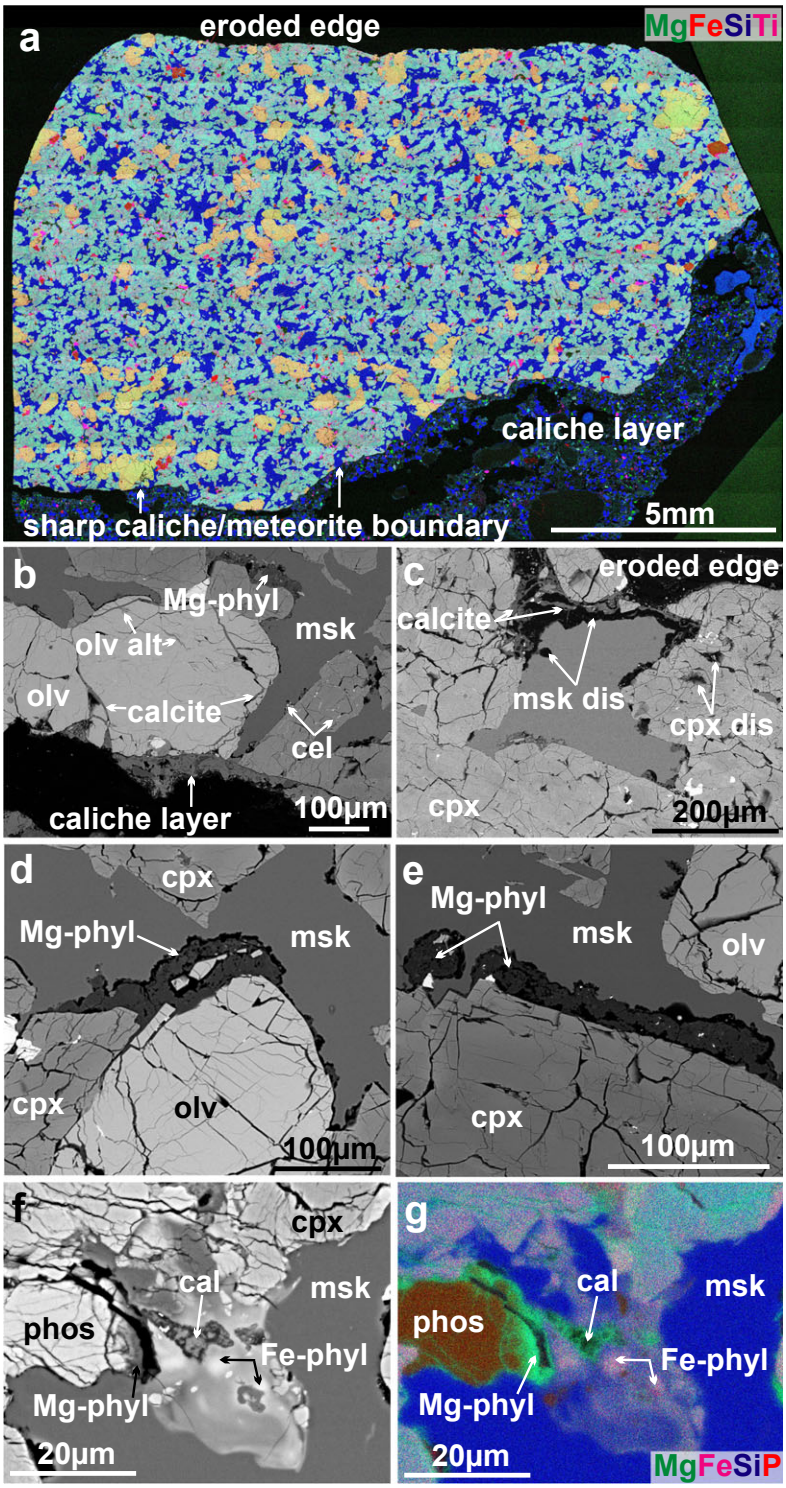

Fig. 1. False-color X-ray (a, g) and BSE images (b–f) of Dhofar 019 thin-section 610-A. The full thin-section false-color image (Mg = green; Fe = red; Si = blue; Ti = pink) shows olivine (olv) in yellow/lime green, clinopyroxene (cpx) in green, maskelynite (msk) in blue, magnetite in red, and ilmenite in pink (a). A terrestrial caliche layer is clearly visible at the edge of this thin-section (a, b). Maskelynite dissolution is mostly present at the boundaries of olivine/clinopyroxene phenocrysts and maskelynite, and is commonly associated with Mg-rich phyllosilicate (Mg-phyl) and calcite (b–e). Phosphate (phos) is present in maskelynite, and can also be altered (f–g). (Color figure can be viewed at wileyonlinelibrary.com.)

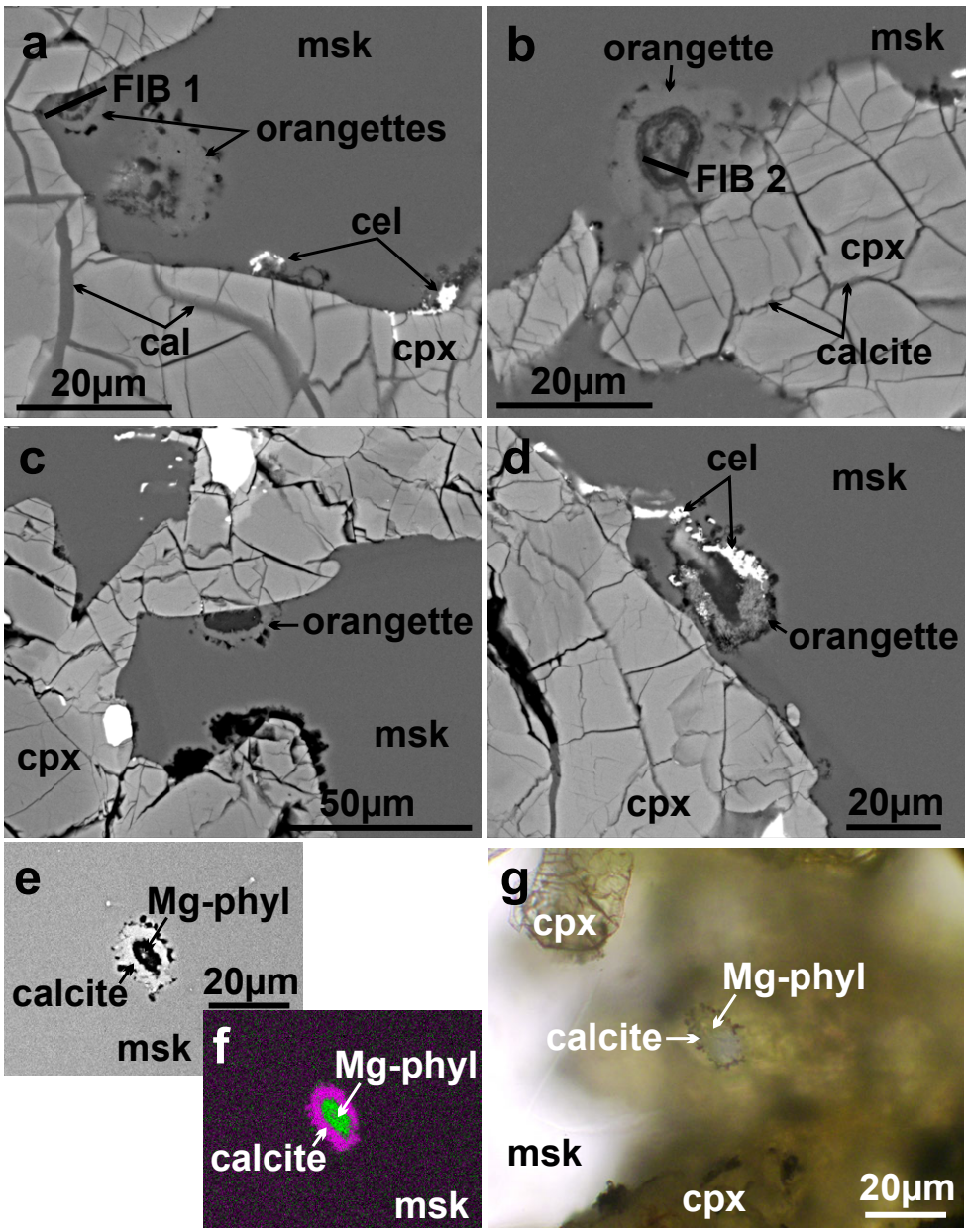

Fig. 2. Electron backscattered SEM images of orangette alteration in Dhofar 019. Calcite (cal) forms the lighter gray layers of each orangette, and Mg-phyllosilicate (phyl) is the darker layers. A number of orangettes contain multiple layers of phyllosilicate and calcite (a, b), and some contain celestine (cel) and barite (a, d). The locations of FIB-sections 1 (a) and 2 (b) are shown. Orangettes are associated with clinopyroxene (cpx) or olivine grain boundaries with maskelynite (msk), or fractures within maskelynite (see Fig. 3). In SEM images, some orangettes appear to be completely hosted within maskelynite (e, f), but optical microscope images (ppl) show connections to fractures or mineral boundaries beneath the sample surface (g). False-color X-ray image (f) shows Ca as pink and Mg as green. Calcite is commonly present as veins in the cracks of associated clinopyroxene. (Color figure can be viewed at wileyonlinelibrary.com.)

2b). In addition, the orangettes of FIB-section 2 appeared to be crosscut by calcite veins extending from within the neighboring clinopyroxene phenocryst. Both FIB-sections show a complex intergrowth of calcite and phyllosilicate, with the two phases commonly intermixed at submicron scales.

FIB-section 1 shows almost the entire orangette cross section from maskelynite to calcite, then a mixed layer of calcite and phyllosilicate, and pure phyllosilicate at the center. The presence of maskelynite is confirmed by the absence of a diffraction pattern for a crystalline phase (Fig. 4a). Calcite commonly has a

Table 1. Dhofar 019 representative mineral chemistry (EDX analyses, wt%).

Mineral	SiO_2	TiO_2	Al_2O_3	FeO	MnO	MgO	CaO	Na_2O	K_2O	SrO	BaO	P_2O_5	SO_2	Total
Clinopyroxene	51.26	0.18	1.01	22.44	0.73	16.90	5.57	0.09	0.01	na	na	nd	nd	98.13
Olivine	33.89	0.07	0.17	44.96	0.70	19.44	0.50	0.16	nd	na	na	0.06	0.05	99.98
Maskelynite	52.14	0.10	29.52	0.58	nd	0.09	12.98	3.96	0.16	na	na	nd	0.03	99.51
Quartz (caliche layer)	100.16	nd	nd	nd	nd	0.01	0.03	0.04	nd	na	na	nd	0.12	100.15
Celestine $SrSO_4$	6.32	0.08	2.87	0.89	0.15	1.11	5.81	0.51	0.04	46.64	2.76	nd	34.05	101.05
Barite $(Ba,Sr)SO_4$	5.02	nd	2.58	1.39	nd	0.84	1.19	0.35	0.07	16.12	39.00	nd	32.64	99.03
Barite $BaSO_4$	0.25	0.26	0.14	nd	nd	0.08	nd	0.11	0.05	0.82	65.54	0.08	33.69	100.73
Mg-phyllosilicate	42.25	0.17	11.68	0.94	0.13	25.62	0.93	0.10	0.25	na	na	0.11	0.24	82.42
Mg-phyllosilicate	40.36	0.16	15.09	0.63	0.02	22.53	2.94	0.13	0.26	na	na	0.55	0.52	83.19
Taylor et al. (2002)														
Mg-smectite	41.70	0.07	14.5	0.95	0.08	24.50	1.72	<0.03	<0.03	na	na	nd	na	83.60
Fe-smectite	42.70	0.34	0.64	13.9	0.44	14.70	3.37	0.06	<0.03	na	na	nd	na	76.30

pure $CaCO_3$ composition, with very little Mg and Na contribution, and no Fe. However, some areas near calcite/phyllosilicate boundaries do contain higher Na abundances (9.33 wt% in one case), as well as appreciable F (up to 3.80 wt%), although the two do not appear to be correlated. The source of Na could be maskelynite, although this is unlikely to produce such high Na abundances. Intergrowth with the Na-carbonate natron is another possibility. Fluorine could be sourced from the dissolution of apatite. However, F is present in both FIB-sections, neither of which were cut from areas with associated apatite grains.

Phyllosilicate throughout most of FIB-sections 1 and 2 has an Mg-, Al-rich composition, similar to the Mg-smectite reported by Taylor et al. (2002), and corresponding to the composition of Mg-rich saponite (Fig. 5). Iron-rich phyllosilicate was not detected in either FIB-section, and in fact was only detected in one place in thin-section 610-A (Figs. 1f and 1g). In most areas, phyllosilicate fringes are poorly ordered, forming isolated fringe "packets" that are misoriented relative to one another. Diffraction rings are evident in these areas, but not diffraction patterns, indicating a low degree of crystallinity (Fig. 4e). Ordered fringes were detected in one area of FIB-section 1, with basal spacings of 7 Å. These narrow spacings are typical of either kaolinite or serpentine rather than smectite, which has basal spacings of 10–15 Å (Deer et al. 1966). Based on the Mg- and Al-rich composition of the surrounding material, the fringes probably represent serpentine, somewhere in the middle of the serpentine-amesite ($Mg_2Al[AlSiO_5](OH)_4$) solid solution. However, the chemical composition of this exact area was not analyzed (Fig. 4b), so it is possible that it is compositionally anomalous (e.g., pure Mg serpentine).

FIB-section 2 samples an orangette with central poorly ordered Mg-saponite, surrounded by alternating layers of calcite and Mg-saponite, underlain by clinopyroxene. The whole orangette is not represented in this FIB-section, as the outer calcite layer and one side of the outer saponite layer were not included (Figs. 2b and 4e). Calcite and Mg-saponite compositions are similar to those of FIB-section 1, but no lattice fringes could be resolved within the saponite. The lack of fringes suggests that the phyllosilicate in this orangette is more poorly crystalline than that in FIB-section 1, although diffraction rings are still evident. Beam damage was observed on FIB-section 1, where fringes degraded within a few seconds of imaging, and nanoporous textures developed. Therefore, it is possible that some phyllosilicate fringes were originally present in the FIB-section 2, but were amorphized by the electron beam before they could be imaged.

Clinopyroxene exhibits well-preserved ladder dislocations, caused by shock pressure (Fig. 4e). Conversely, dislocations are not visible in the calcite of either FIB-section, although shock ladder dislocations (among other types) have been shown to be relatively well preserved in carbonates (Langenhorst et al. 2003).

DISCUSSION

Compositional Comparisons of Dhofar 019 Alteration with That in Other Martian Meteorites

Martian smectite occurs within alteration veins in the nakhlite group of meteorites, commonly in the form of poorly ordered Fe-rich saponite (Fig. 5). The phyllosilicate analyzed in Dhofar 019 does have a chemical composition corresponding to saponite ($(Ca_{0.25}(Mg,Fe)_3((Si,Al)_4O_{10})(OH)_2{\cdot}n(H_2O))$), but is much more Mg-rich than the nakhlite saponite, even including the Fe-rich smectite reported by Taylor et al. (2002). An Mg-rich composition is more closely aligned with typical terrestrial saponite (Fig. 5). It could be argued that because the Dhofar 019 phyllosilicate is found in maskelynite, whereas that of the nakhlites is found within olivine, a direct comparison is invalid. However, the composition of the former indicates that it is formed

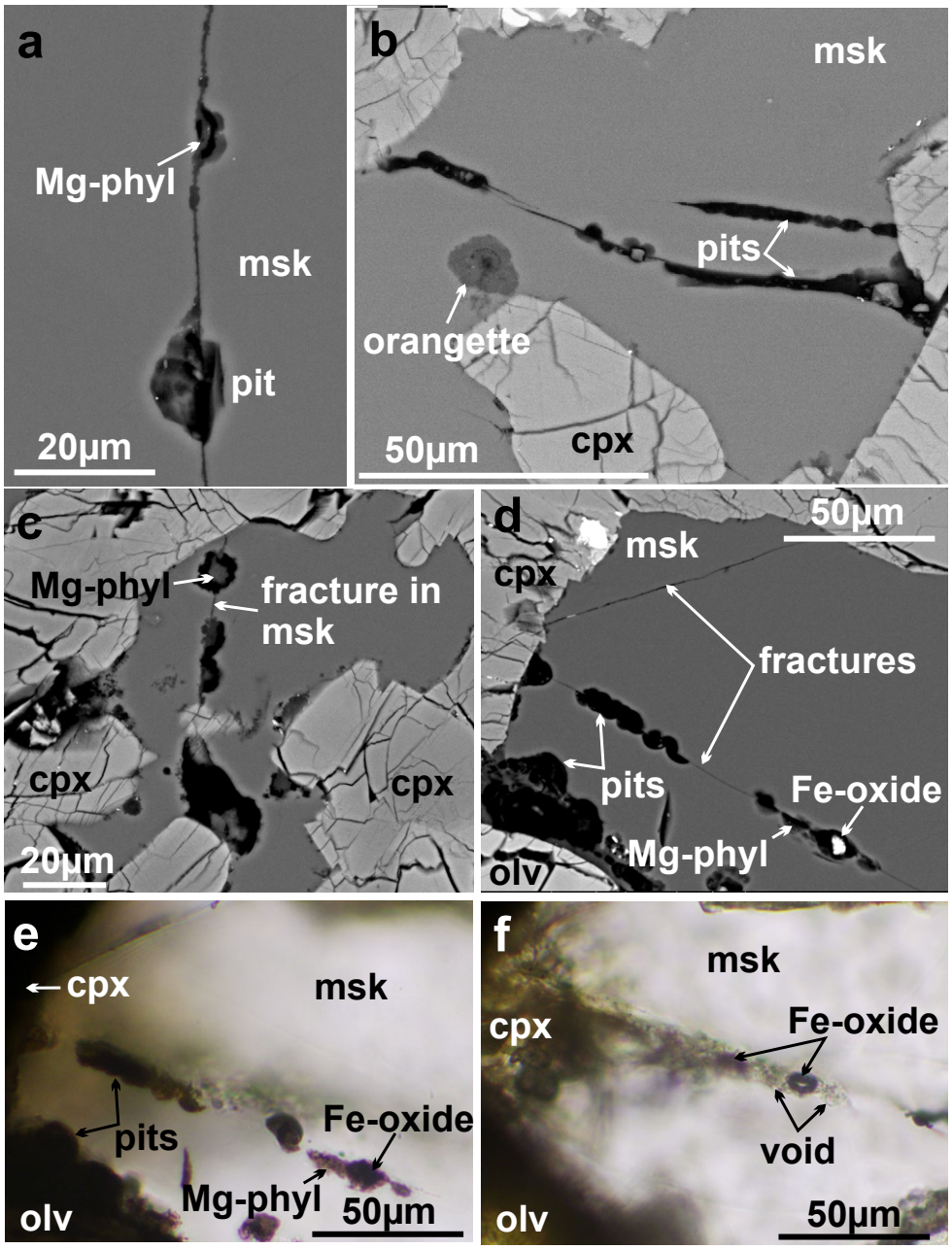

Fig. 3. Electron backscattered SEM images (a–d) and optical microscope images (e, f) of fracturing in maskelynite. Electron backscattered images show as semispherical pits along fractures, indicative of maskelynite dissolution. These pits commonly contain secondary alteration in the form of Mg-phyllosilicate (Mg-phyl) (a, c), but some contain no alteration (b, d). Fe-oxide (probably hematite) is associated with phyllosilicate (e, f). cpx = clinopyroxene; olv = olivine. (Color figure can be viewed at wileyonlinelibrary.com.)

via the dissolution of several minerals including olivine and clinopyroxene, not just maskelynite. For a broader comparison, the composition of amorphous material from the soil at Gale crater is also plotted in Fig. 5. This soil represents a good estimate of the average composition for this type of alteration on Mars, unrestricted to a certain lithology or mineral. The low-Mg and high-Fe content of this amorphous soil alteration contrasts with the Mg-phyllosilicate of Dhofar 019, suggesting that the latter does not have a Martian origin.

The presence of almost pure $CaCO_3$ calcite, celestine, and barite within the orangettes is consistent with a terrestrial origin. The calcite almost was certainly formed via fluid transport of Ca and HCO_3 into the meteorite from the surrounding caliche soil at the

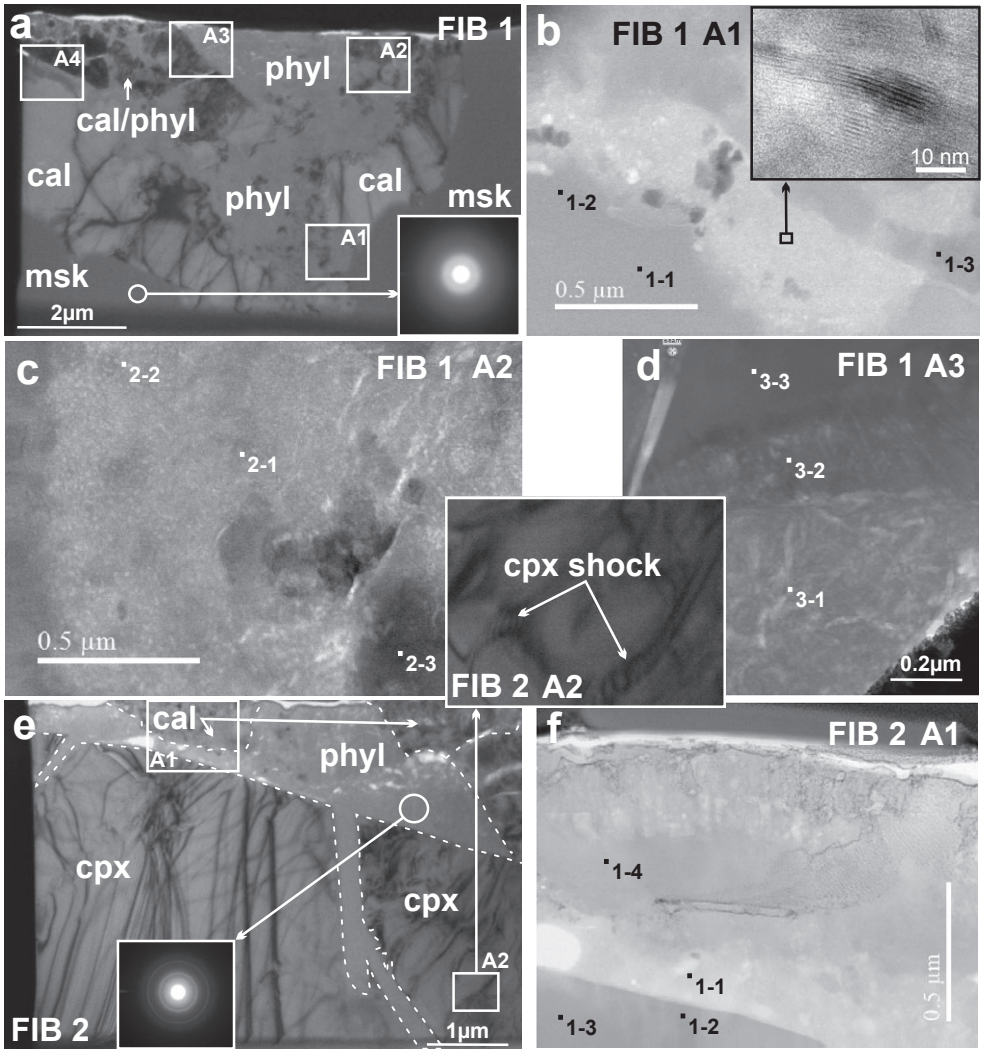

Fig. 4. Bright-field (a, inset b, e) and high-angle annular dark-field (b–d, f) scanning TEM images of FIB-sections 1 (a–d) and 2 (e, f) taken from Dhofar 019 thin-section 610-A. Locations of EDX spots on the samples are marked by values 1-1 etc., with corresponding chemical compositions highlighted in Table 2. Fringe widths of 7 Å (b, inset) correspond to serpentine in one area.

landing site in Oman. The presence of more abundant calcite and celestine/barite deposits toward the outer edges of the sample, as well as the absence of shock dislocation features within FIB-1 and FIB-2 calcite, support a terrestrial origin. Martian carbonate typically contains much higher concentrations of Fe and Mg (e.g., Niles et al. 2012). For example, ALH 84001 carbonate rosettes have an average composition of $(Fe_{29}Mg_{60}Ca_{11})CO_3$ (e.g., Mason et al. 1992), with zonation between Fe- and Mg-rich carbonates (Harvey and McSween 1996; Gleason et al. 1997; McKay and Lofgren 1997; Scott et al. 1997, 1998; Niles et al. 2012). Compositionally pure Martian calcite has yet to be reported, either within meteorites or on the planet's surface (Niles et al. 2012). While it should be noted that this does not mean there is no pure calcite on Mars, it would be highly coincidental for the first evidence of such calcite to be found within Dhofar 019—a caliche-coated meteorite with a terrestrial exposure age of 0.34 ± 0.04 Ma (Nishiizumi et al. 2002). The terrestrial origin of caliche layers and calcite veins within Martian hot desert meteorites has been discussed in detail by Coulson et al. (2007), Grady et al. (2007), Treiman and Irving (2008), and Tomkinson et al. (2015). Celestine and barite are only found within 3 mm of the caliche-coated sample edge, confirming their terrestrial origin. The presence of these evaporitic minerals within the central layers of a number of orangettes confirms that these structures must have formed in the desert of Northwest Africa.

Fluorite was not detected during SEM or TEM analyses, but high concentrations of F within the calcite and phyllosilicate zones were found within both FIB sections. As the F seems to be present in phyllosilicate,

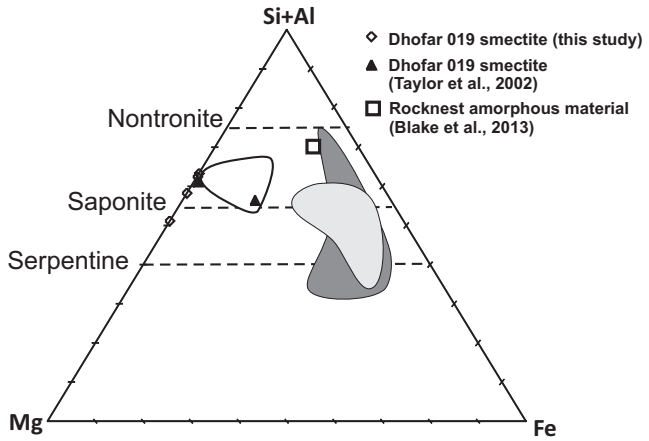

Fig. 5. Phyllosilicate ternary plot comparing the chemical composition of Dhofar 019 poorly ordered phyllosilicate with nakhlite iddingsite and amorphous Martian soil material. Ratios were calculated from atom% values. Nakhlite iddingsite data were collected from Lafayette, Nakhla, Governador Valadares, Yamato-000593, and Yamato-000749 (light gray envelope; Changela and Bridges 2011; Hicks et al. 2014), and the four Miller Range nakhlites (dark gray envelope; Hallis et al. 2014; Hicks et al. 2014). Rocknest (Gale Crater) amorphous material from the Martian soil (Blake et al. 2013) and typical terrestrial saponite compositions (white envelope; Changela and Bridges [2011] and references therein) are also plotted for comparison.

and calcite close to the boundary with phyllosilicate, it is probably a contaminant brought into the alteration area from elsewhere. The dissolution of apatite is a possibility (e.g., McCubbin et al. 2012), but F is present in both FIB-sections, neither of which were cut from areas with associated apatite grains. It is unlikely that nonlocal apatite contributed significantly to the F content of calcite and phyllosilicate in these FIB-sections, as apatite is a minor mineral in Dhofar 019, which is not extensively altered (Figs. 1f and 1g show the only apatite found with observable alteration). Maskelynite does not contain appreciable F. It therefore seems probable that at least some of the F was sourced externally, from the terrestrial hot desert environment. As fluorite is commonly associated with celestine, barite, and calcite (Deer et al. 1966), it seems logical that F was brought into the meteorite, along with Sr, Ba, Ca, and the Cl detected in FIB-1 area 3 phyllosilicate, via water infiltration during the stones' long residence in Northwest Africa. The Na content of calcite, and to a lesser extent phyllosilicate, could be due to the concentration of Na from the replacement of maskelynite (containing ~4 wt% Na_2O). However, it too could have been brought in from the terrestrial desert environment—halite is common in this environment (e.g., Glennie 1987). The higher concentration of Na in calcite compared with phyllosilicate indicates it may be present as an intergrowth of Na-carbonate (natron).

Formation of Dhofar 019 Orangettes in a Terrestrial Environment

Saponite commonly forms in cavities and veins within terrestrial basalts (e.g., Deer et al. 1966). Therefore, the orangettes in Dhofar 019 may have formed via aqueous transport of the cations Mg and Fe, along with trace amounts of Na, P, S, K, Ti, and Mn (Tables 1 and 2), from the surrounding olivine, clinopyroxene, and maskelynite into cracks and cavities already in existence in the maskelynite of this meteorite. The abundance of Mg (and rarely Fe) in Dhofar 019 phyllosilicate are indicative of the amount of olivine and clinopyroxene weathering that has occurred within the meteorite. Weathering of olivine is evident along internal fractures, and clinopyroxene shows dissolution at the meteorite's edges (Fig. 1c). Weathering of these minerals provides abundant Mg and Fe cations in solution. Maskelynite dissolution appears to commence from grain boundaries and preexisting fractures in thin-section 610-A, creating pits (Fig. 3). Some of these pits remain empty, with sharp edges (e.g., Figs. 3b and 3d), whereas some exhibit phyllosilicate replacement of the surrounding maskelynite, resulting in diffuse void edges (e.g., Figs. 3a and 3c). These diffuse edges probably signify a shift to direct maskelynite alteration, rather than two-step dissolution and later deposition. Maskelynite already contains Si and Al, thus aqueous alteration by an Mg-rich fluid could produce the Mg-saponite compositions reported. In contrast, Ca appears to have been brought in from the terrestrial environment rather than as a product of meteorite weathering—i.e., from the caliche soil. Calcite in Dhofar 019 is depositional, filling pits and cracks. Where calcite is the outermost layer in the orangette, its boundary with maskelynite is sharp, emphasizing its depositional nature—it does not replace maskelynite as phyllosilicate does (e.g., Fig. 4a).

Compositionally, the orangettes are similar to the larger areas of alteration (e.g., Figs. 1d and 1e), indicating that these layered structures represent the onset of terrestrial alteration within maskelynite. The initial growth of an orangette can start with phyllosilicate or calcite deposition in a preexisting maskelynite void space. Where phyllosilicate is the outermost layer, direct alteration and replacement of maskelynite occur and a diffuse edge is commonly formed (illustrated in Figs. 3a and 3c). We conclude that the apparent offsetting of a smectite orangette reported by Taylor et al. (2002) was probably produced by the growth of hemispherical dissolution pits on

Table 2. Mineral chemistry from FIB sections (EDX wt%, representative analyses).

	Mineral	Si	Al	Fe	Mg	Ca	Na	K	C	F	Cl	O	Total
Dhofar 019 FIB-1													
Area 1													
EDS1-1	Diaplectic glass	50.8	4.6			0.46			0.45			43.69	100
EDS1-2	Maskelynite	32.7	19.37			6.83	3.1					37.99	99.99
EDS1-3	Calcite					45.43			9.51			45.06	100
Area 2													
EDS2-1	Mg-phyllosilicate	24.85	7.99		17.3	1.24	0.59	0.97	2.24			44.83	100.01
EDS2-2	Mg-phyllosilicate	24.81	8.04		16.66	1.22		0.29	1.84	1.45		45.69	100
EDS2-3	Calcite	2.46	0.97		1.68	37.12	1.01		8.25			48.51	100
Area 3													
EDS3-1	Mg-phyllosilicate	17.58	9.25		22.48	0.2			1.02	1.98	0.42	47.06	99.99
EDS3-2	Calcite				0.33	37.84	0.8		8.42	2.76		49.84	99.99
EDS3-3	Calcite					42.35	0.88		10.86			45.9	99.99
Area 4													
EDS4-1	Calcite				0.54	43.63			10.32			45.51	100
EDS4-2	Calcite/natron mix?					31.27	9.33		11.92	3.89		43.6	100.01
EDS4-3	Calcite				0.82	41.43	1.31		10.17			46.28	100.01
Dhofar 019 FIB-2													
Area 1													
EDS1-1	Mg-phyllosilicate	23.88	6.5		19.02		0.77		1.07			48.76	100
EDS1-2	Clinopyroxene	34.55		6.22	11.2	9.24						38.78	99.99
EDS1-3	Clinopyroxene	32.9		5.86	11.9	9.37						39.98	100.01
EDS1-4	Calcite					36.96	1.89		9.5			51.66	100.01
Area 2													
EDS2-2	Calcite/phyllosilicate mix	9.11	4.78		8.07	11.6	4.36		6.88	5.66		49.53	99.99
EDS2-3	Clinopyroxene	31.55	0.68	7.55	10.7	9.95						39.56	99.99

either side of a maskelynite fracture, followed by later deposition of phyllosilicate.

It is possible that the pits and large void spaces within Dhofar 019 maskelynite once contained a preexisting Martian alteration assemblage, which has been dissolved and reworked by terrestrial weathering. Such phases would be susceptible to aqueous alteration. However, if this were the case, compositional clues might be expected that are not evident (e.g., high sulfur content in Mg-phyllosilicate and higher Fe content in both carbonate and phyllosilicate).

Dhofar 019 is one of the most terrestrially weathered Martian meteorites, with a terrestrial exposure age of 0.34 ± 0.04 Ma (Nishiizumi et al. 2002). This is undoubtedly the reason why this meteorite contains such abundant alteration. However, it is not the only meteorite to contain such alteration. Although the term "orangette" has only previously been used to describe alteration in Dhofar 019, the shergottite Sayh al Uhaymir (SaU) 094 is described as having "bright orange secondary Mg-Fe-Si silicate alteration found in association with melted areas" (Gnos et al. 2002), with a similar texture to the alteration in Dhofar 019. This alteration in SaU 094 was interpreted as terrestrial in origin.

Implications of the Absence of Martian Alteration Minerals in the Shergottites

We conclude that all of the calcite and phyllosilicate in Dhofar 019 is terrestrial, implying none of the shergottites contain products of low-temperature aqueous alteration on Mars (Tissint may have experienced deuteric alteration; Hallis et al. 2017). The absence of these minerals in the largest group of Martian meteorites indicates that they were never exposed to liquid water during their residence on Mars. Based on Pb-Pb isotope ratios, it has been suggested that the shergottites are the oldest group of Martian meteorites, having crystallized at ~4.3 Ga (Bouvier et al. 2008). In addition, the <5 Myr old and 55-km wide Mojave crater, which formed in terrain with an age of 4.3 Ga, has recently been suggested as the shergottite source crater (Werner et al. 2014). However, it seems unlikely that the shergottites could have been resident on Mars for 4.3 billion years without exposure to liquid water, especially as the Noachian and pre-Noachian (4.5–3.7 Ga) periods in Martian geological history are known to have hosted abundant liquid water at the surface, even possibly a northern ocean (e.g., Head et al. 1999; Jakosky and Phillips 2001). Therefore, the

lack of aqueous alteration minerals indicates that the much younger crystallization ages of between 165 and 575 Ma are more likely for the shergottites. This younger shergottite age is also supported by baddeleyite U-Pb ages from NWA 5298 (Moser et al. 2013). Even with this younger age, the shergottites have still been present on the Martian surface for hundreds of millions of years without being exposed to water. This conclusion suggests that current Martian water is not only transient (McEwen et al. 2011) but also isolated to certain depths and regions of the planet.

Acknowledgments—The research leading to these results has received funding from the People Programme (Marie Curie Actions) of the European Union's Seventh Framework Programme (FP7/2007-2013) under REA grant agreement no. 624137. We also acknowledge funding from the UK STFC through grant ST/N000846/1. Peter Chung and Sam McFadzean are thanked for their help with SEM and TEM data collection, respectively, along with Prof. John Bridges and Prof. Adrian Brearley for their helpful comments and suggestions during the review process.

Editorial Handling—Dr. Adrian Brearley

REFERENCES

Agee C. B., Wilson N. V., McCubbin F. M., Ziegler K., Polyak V. J., Sharp Z. D., Asmerom Y., Nunn M. H., Shaheen R., Thiemens M. H., Steele A., Fogel M. L., Bowden R., Glamoclija M., Zhang Z., and Elardo S. M. 2013. Unique meteorite from Early Amazonian Mars: Water-rich basaltic breccia Northwest Africa 7034. *Science* https://doi.org/10.1126/science.1228858.

Blake D. F., Morris R. V., Kocurek G., Morrison S. M., Downs R. T., Bish D., Ming D. W., Edgett K. S., Rubi D., Goetz W., Madsen M. B., Sullivan R., Gellert R., Campbell I., Treiman A. H., McLennan S. M., Yen A. S., Grotzinger J., Vaniman D. T., Chipera S. J., Achilles C. N., Rampe E. B., Sumner D., Meslin P.-Y., Maurice S., Forni O., Gasnault O., Fisk M., Schmidt M., Mahaffy P., Leshin L. A., Glavin D., Steele A., Freissinet C., Navarro-González R., Yingst R. A., Kah L. C., Bridges N., Lewis K. W., Bristow T. F., Farmer J. D., Crisp J. A., Stolper E. M., Des Marais D. J., and Sarrazin P. 2013. Curiosity at Gale Crater, Mars: Characterization and analysis of the Rocknest sand shadow. *Science* 341:1239505.

Borg L. E., Nyquist L. E., Reese Y., Wiesmann H., Shih C.-Y., Taylor L. A., and Ivanova M. 2001. The age of Dhofar 019 and its relationship to the other Martian meteorites (abstract #1144). 32nd Lunar and Planetary Science Conference. CD-ROM.

Bouvier A., Blichert-Toft J., Vervoort J. D., Gillet P., and Albarède F. 2008. The case for old basaltic shergottites. *Earth and Planetary Science Letters* 266:105–124.

Brandon A. D., Walker R. J., Putchel I. S., and Irving A. J. 2008. Re-Os isotopic systematics of the shergottite 'depleted' end-member. 39th Lunar and Planetary Science Conference. CD-ROM.

Brandon A. D., Putchel I. S., Walker R. J., Day J. M. D., Irving A. J., and Taylor L. A. 2012. Evolution of the Martian mantle inferred from the ^{187}Re-^{187}Os isotope and high siderophile element systematics of the Shergottite meteorites. *Geochimica et Cosmochimica Acta* 76:206–235.

Brennecker G. A., Borg L. E., and Wadhwa M. 2014. Insights into the Martian mantle: The age and isotopics of the meteorite fall Tissint. *Meteoritics & Planetary Science* 49:412–418.

Bridges J. C. and Grady M. M. 2000. Evaporite mineral assemblages in the nakhlite (Martian) meteorites. *Earth and Planetary Science Letters* 176:267–279.

Changela H. G. and Bridges J. C. 2011. Alteration assemblages in the nakhlites: Variation with depth on Mars. *Meteoritics & Planetary Science* 45:1847–1867.

Christensen P. R. 2003. Formation of recent Martian gullies through melting of extensive water-rich snow deposits. *Nature* 422:45–48.

Coulson I. M., Beech M., and Nie W. 2007. Physical properties of Martian meteorites: Porosity and density measurements. *Meteoritics & Planetary Science* 42:2043–2054.

Deer W. A., Howie R. A., and Zussman J. 1966. *An introduction to the rock forming minerals*. London: Longman Group Limited.

Gleason J. D., Kring D. A., Hill D. H., and Boynton W. V. 1997. Petrography and bulk chemistry of Martian orthopyroxenite ALH 84001: Implications for the origin of secondary carbonates. *Geochimica et Cosmochimica Acta* 61:3503–3512.

Glennie K. W. 1987. Desert sedimentary environments, present and past: A summary. *Sedimentary Geology* 50:135–165.

Gnos E., Hofmann B., Franchi I. A., Al-Kathiri A., Houser M., and Moser L. 2002. Sayh al Uhaymir 094: A new Martian meteorite from the Oman desert. *Meteoritics & Planetary Science* 37:835–854.

Gooding J. L., Wentworth S. J., and Zolensky M. E. 1991. Aqueous alteration of the Nakhla meteorite. *Meteoritics* 26:135–143.

Grady M. M., Anand M., Gilmour M. A., Watson J. S., and Wright I. P. 2007. Alteration of the Nakhlite Lava Pile: Was water on the surface, seeping down, or at depth, percolating up? Evidence (such as it is) from carbonates (abstract #1826). 38th Lunar and Planetary Science Conference. CD-ROM.

Grossman J. N. 2000. The Meteoritical Bulletin, No. 84. *Meteoritics & Planetary Science* 35:A199–225.

Hallis L. J. 2013. Alteration assemblages in the Miller Range and Elephant Moraine regions of Antarctica: Comparisons between terrestrial igneous rocks and Martian meteorites. *Meteoritics & Planetary Science* 48:165–179.

Hallis L. J. and Taylor G. J. 2011. Comparisons of the four Miller Range nakhlites, MIL 03346, 090030, 090032 and 090136: Textural and compositional observations of primary and secondary mineral assemblages. *Meteoritics & Planetary Science* 46:1787–1803.

Hallis L. J., Ishii H. A., Bradley J. P., and Taylor G. J. 2014. Transmission electron microscope analyses of alteration phases in Martian meteorite MIL 090032. *Geochimica et Cosmochimica Acta* 134:275–288.

Hallis L. J., Huss G. R., Nagashima K., Taylor G. J., Stöffler D., Smith C. L., and Lee M. R. 2017. Effects of shock and Martian alteration on Tissint hydrogen isotope ratios and water content. *Geochimica et Cosmochimica Acta* 200:280–294.

Harvey R. P. and McSween H. Y. 1996. A possible high-temperature origin for the carbonates in Martian meteorite ALH 84001. *Nature* 382:49–51.

Head J. W., Hiesinger H., Ivanov M. A., Kreslavsky M. A., Pratt S., and Thomson B. J. 1999. Possible ancient oceans on Mars: Evidence from Mars Orbiter Laser Altimeter. *Science* 286:2134–2137.

Hicks L. J., Bridges J. C., and Gurman S. J. 2014. Ferric saponite and serpentine in the nakhlite Martian meteorites. *Geochimica et Cosmochimica Acta* 136:194–210.

Jakosky B. M. and Phillips R. J. 2001. Mars' volatile and climate history. *Nature* 412:237–244.

Langenhorst F., Boustie M., Deutsch A., Hornemann U., Matignon C., Migault A., and Romain J. P. 2003. Experimental techniques for the simulation of shock metamorphism: A case study on calcite. In *High-pressure shock compression of solids V: Shock wave and high pressure phenomena*, edited by Davison L., Horie Y., and Sekine T. New York: Springer. pp. 1–27.

Lee M. R., Bland P. A., and Graham G. 2003. Preparation of TEM samples by focused ion beam (FIB) techniques: Applications to the study of clays and phyllosilicates in meteorites. *Mineralogical Magazine* 67:581–592.

Mason B., MacPherson G. J., Score R., Martinez R., Satterwhite C., Schwarz C., and Gooding J. L. 1992. Descriptions of stony meteorites. In *Field and laboratory investigations of Antarctic meteorites collected by the United States expeditions 1985–1987*, edited by Marvin U. B. and MacPherson G. J. *Smithsonian Contributions to Earth Sciences* 30:17–35.

McCubbin F. M., Hauri E. H., Elardo S. M., Van der Kaaden K. E., Wang J., and Shearer C. K. Jr. 2012. Hydrous melting of the Martian mantle produced both depleted and enriched shergottites. *Geology* 40:683–686.

McEwen A., Ojha L., Dundas C. M., Mattson S. S., Byrne S., Wray J. J., Cull S. C., Murchie S. L., Thomas N., and Gulick V. G. 2011. Seasonal flows on warm Martian slopes. *Science* 333:740–743.

McKay G. A. and Lofgren G. E. 1997. Carbonates in ALH 84001: Evidence for kinetically controlled growth. Proceedings, 27th Lunar and Planetary Science Conference. pp. 921–922.

Mittlefehldt D. W. and Lindstrom M. M. 1994. Geochemical evidence for mixing of three components in Martian orthopyroxenite ALH 84001 (abstract). *Meteoritics* 29:504.

Moser D. E., Chamberlain K. R., Tait K. T., Schmitt A. K., Darling J. R., Barker I. R., and Hyde B. C. 2013. Solving the Martian meteorite age conundrum using micro-baddeleyite and launch-generated zircon. *Nature* 499:454–457.

Muttik N., McCubbin F. M., Keller L. P., Santos A. R., McCutcheon W. A., Provencio P. P., Rahman Z., Shearer C. K., Boyce J. W., and Agee C. B. 2014. Inventory of H_2O in the ancient Martian regolith from Northwest Africa 7034: The important role of Fe oxides. *Geophysical Research Letters* 41:8235–8244.

Niles P. B., Catling D. C., Berger G., Chassefière E., Ehlmann B. L., Michalski J. R., Morris R., Ruff S. W., and Sutter B. 2012. Geochemistry of carbonates on Mars: Implications for climate history and nature of aqueous environments. *Space Science Reviews* 174:301–328.

Nishiizumi K., Okazaki R., Park J., Nagao K., Masarik J., and Finkel R. C. 2002. Exposure and terrestrial histories of Dhofar 019 Martian meteorite. 33rd Lunar and Planetary Science Conference. CD-ROM.

Nishiizumi K., Caffee M. W., and Irving A. J. 2012. Exposure history of Tissint: Evidence for 1.1 million year launch pairing with other depleted olivine-phyric shergottites (abstract #5349). 75th Annual Meteoritical Society Meeting #5349. Meteoritics & Planetary Science 47.

Nyquist L. E., Bogard D. D., Shih C.-Y., Greshake A., Stöffler D., and Eugster O. 2001. Ages and geologic histories of Martian meteorites. *Chronology and Evolution of Mars, Space Sciences Series of ISSI* 12:105–164.

Ojha L., Wilhelm M. B., Murchie S. L., McEwen A. S., Wray J. J., Hanley J., Massé M., and Chojnacki M. 2015. Spectral evidence for hydrated salts in recurring slope lineae on Mars. *Nature Geoscience* 8:829–832.

Romanek C. S., Grady M. M., Wright I. P., Mittlefehldt D. W., Socki R. A., Pillinger C. T., and Gibson E. K. 1994. Record of fluid rock interactions on Mars from the meteorite ALH 84001. *Nature*, 372:655–657.

Scott E. R. D. 1999. Origin of carbonate-magnetite-sulfide assemblages in Martian meteorite ALH 84001. *Journal of Geophysical Research* 104:3803–3813.

Scott E. R. D., Yamaguchi A., and Krot A. N. 1997. Petrological evidence for shock melting of carbonates in the Martian meteorite ALH 84001. *Nature* 387:377–379.

Scott E. R. D., Krot A. N., and Yamaguchi A. 1998. Carbonates in fractures of Martian meteorite Allan Hills 84001: Petrologic evidence for impact origin. *Meteoritics & Planetary Science* 33:709–719.

Shukolyukov Y. A., Nazariv M. A., and Schultz L. 2002. A new Martian meteorite: The Dhofar 019 shergottite with an exposure age of 20 million years. *Solar System Research* 36:125–135.

Taylor L. A., Nazarov M. A., Shearer C. K., McSween H. Y. Jr., Cahill J., Neal C. R., Ivanova M. A., Barsukova L. D., Lentz R. C., Clayton R. N., and Mayeda T. K. 2002. Martian meteorite Dhofar 019: A new shergottite. *Meteoritics & Planetary Science* 37:1107–1128.

Tomkinson T., Lee M. R., Mark D. F., and Smith C. L. 2013. Sequestration of Martian CO_2 by mineral carbonation. *Nature Communications* 4:2662.

Tomkinson T., Lee M. R., Mark D. F., Dobson K. J., and Franchi I. A. 2015. The Northwest Africa (NWA) 5790 meteorite: A mesostasis-rich nakhlites with little or no Martian aqueous alteration. *Meteoritics & Planetary Science* 50:287–304.

Treiman A. H. and Irving A. J. 2008. Petrology of Martian meteorite Northwest Africa 998. *Meteoritics & Planetary Science* 43:829–854.

Treiman A. H. and Romanek C. S. 1998. Bulk and stable isotopic compositions of carbonate minerals in Martian meteorite Allan Hills 84001: No proof of high formation temperature. *Meteoritics & Planetary Science* 33:737–742.

Wentworth S. J. and Gooding J. L. 1994. Carbonates and sulphates in the Chassigny meteorite: Further evidence for aqueous chemistry on the SNC parent body. *Meteoritics* 29:860–863.

Werner S. C., Ody A., and Poulet F. 2014. The source crater of Martian shergottite meteorites. *Science* 343:1343–1346.